Quarterly Fusion Theory Milestone Report for 2006 Quarter 1

(Submitted 12/31/05, revised 01/09/06)

S.E. Kruger[1], D.D. Schnack[2], H. R. Strauss[3], L. Sugiyama[4], D. Brennan[4], J. Breslau[5], S.C Jardin[5], W. Park[5], S.P. Smith[5]

I. Executive Summary

In this report, we present the successful completion of the 2006 Q1 milestone, namely: an n=0 steady-state near the 2005 700 eV equilibria was found. Because the H-mode equilibria used in the ELM studies are the most challenging equilibria ever used by nonlinear initial-value, extended MHD codes, details on the numerical challenges faced by both NIMROD and M3D are presented. This quarterly milestone motivated new development of the NIMROD code: namely more flexibility in source specification and run time operation. These developments will allow NIMROD more flexibility in meeting the challenges of subsequent milestones. We also present progress in 2-fluid modeling of ELMs with the M3D code, of generating an adaptive mesh that can adequately resolve the large gradients in the pedestal region, and discuss the implementation of a technique for transferring steady state "stationary" equilibrium from a free boundary transport code to an Extended MHD code.

II. Statement of Problem

At the conclusion of the 2005 ELM milestone, the NIMROD [1] code successfully ran an ELM simulation far into the nonlinear regime allowing for the study of heat flux on the wall. Even in those successful simulations, numerical difficulties occurring at the separatrix occurred well beyond where a "separatrix" could be clearly defined. Because of NIMROD's "separation of equilibrium variables" (to be discussed in Section III.B.), these problems were believed to be associated with how the $n = 0$ steady-state fields are initialized. The M3D [2] code observed similar numerical problems when using the equilibrium as given. Because of these problems, the first quarterly milestone was chosen to investigate the $n = 0$ solutions and determine a more appropriate initialization – one that would prevent numerical issues. The ability to have an appropriate $n = 0$ state as the initial condition will prepare the codes for the more challenging milestones in the coming year.

III. Technical Background

A. Equilibrium Definition

In tokamaks, the plasmas are often quiescent with very little non-symmetric components of the fields. It is the low-frequency, long-wavelength deviations away from this symmetry that is studied with nonlinear, initial-value, extended MHD codes. To study the deviations, extended MHD simulations of large tokamaks generally start with

[1] TechX Corporation
[2] SAIC and U. Wisconsin
[3] Courant Institute of Mathematical Sciences, New York University
[4] Massachusetts Institute of Technology
[5] Princeton University Plasma Physics Laboratory

symmetric fields coming from a Grad-Shafranov equilibrium. As discussed below, the Grad-Shafranov equilibrium is a subset of the steady-state MHD equations. Considerable effort has gone into experimentally reconstructing the symmetric fields based on the Grad-Shafranov model. The most widely-used code for performing this reconstruction is the EFIT code from General Atomics. Because we are interested in nonlinear simulations of ELMs, the equilibrium code used to initialize the code must include the separatrix; i.e., it must be a *free-boundary GS solver*. Beyond EFIT, a widely-used code for this purpose is the TEQ code from LLNL.

To place the initial conditions of the nonlinear initial-value codes in context, we briefly review the extended MHD equations. The extended MHD equations that we are solving are:

Continuity: $$\frac{\partial n}{\partial t} + \nabla \cdot \mathbf{V} = 0 \quad , \tag{1a}$$

Momentum: $$Mn\frac{d\mathbf{V}}{dt} = -\nabla p + \mathbf{J}\times\mathbf{B} - \nabla\cdot\Pi_{visc} - \nabla\cdot\Pi_{gv} - \nabla\cdot\Pi_{\|} \quad , \tag{1b}$$

Gen. Ohm's Law: $$\mathbf{E} = -\mathbf{V}\times\mathbf{B} + \frac{1}{ne}\left[\mathbf{J}\times\mathbf{B} - \nabla p_e - \nabla\cdot\Pi_e\right] + \eta\mathbf{J} \quad . \tag{1c}$$

Energy: $$n_\alpha\left(\frac{\partial T_\alpha}{\partial t} + \mathbf{V}_\alpha \bullet \nabla T_\alpha\right) = (\gamma - 1)\left[\nabla \bullet \mathbf{q}_\alpha + ...\right]. \tag{1d}$$

where ***J*** is the plasma current density, and p is the plasma pressure (total unless subscripted for the species). To form the complete set of evolution equations, we use the "pre-Maxwell equations"; i.e., Maxwell's equations without the displacement current.

Div(B): $$\nabla\cdot\mathbf{B} = 0 \quad , \tag{2a}$$

Ampere's Law: $$\nabla\times\mathbf{B} = \mu_0\mathbf{J} \quad , \tag{2b}$$

Faraday's Law $$\frac{\partial\mathbf{B}}{\partial t} = \nabla\times\mathbf{E} \quad , \tag{2c}$$

The lack of displacement current (and concomitant disregard of Gauss's Law) is the "quasineutrality" approximation, which is $|q_e|n_e = q_i n_i$. This approximation is valid for the low frequencies ($\omega^2 << c^2k^2$) studied in extended MHD.

The form of the generalized Ohm's law (Eq. 1.c) generally distinguishes the commonly used extended MHD. In this document, we will make reference to three models: ideal MHD, resistive MHD, and extended MHD. These are:

Ideal MHD: $$\mathbf{E} = -\mathbf{V}\times\mathbf{B} \tag{3a}$$

Resistive MHD: $$\mathbf{E} = -\mathbf{V}\times\mathbf{B} + \eta\mathbf{J} \quad . \tag{3b}$$

Extended MHD: $$\mathbf{E} = -\mathbf{V}\times\mathbf{B} + \frac{1}{ne}\left[\mathbf{J}\times\mathbf{B} - \nabla p_e - \nabla\cdot\Pi_e\right] + \eta\mathbf{J} \quad . \tag{3c}$$

In addition to neglecting the resistivity, ideal MHD ignores all other dissipative terms (i.e., no viscosity and all terms on right-side of Eq. 1.d. are neglected). Resistive MHD

traditionally has neglected all terms on right-side of Eq. 1.d. although there is no standard nomenclature in the literature.

To derive the "steady-state" solutions of the extended MHD equations, two assumptions are usually made: (1) the diffusive terms operate on time-scales much longer than the "steady-state" and can be neglected, and (2) we consider $n = 0$. The first assumption allows the definition of "steady-state" to be the transport time scale, which is generally much slower than the time scales of the instabilities we wish to study. This is discussed further in Section III.B. Using these assumptions, the relevant equations are:

Continuity: $$\nabla \cdot n_0 \mathbf{V}_0 = 0 \quad , \tag{4a}$$

Momentum: $$m n_0 \mathbf{V}_0 \bullet \nabla_0 \mathbf{V}_0 = -\nabla p_0 + \mathbf{J}_0 \times \mathbf{B}_0 \ , \tag{4b}$$

Gen. Ohm's Law: $$\mathbf{E}_0 + \mathbf{V}_0 \times \mathbf{B}_0 = \frac{1}{n_0 e}\left[\mathbf{J}_0 \times \mathbf{B}_0 - \nabla p_{e0} - \nabla \cdot \Pi_{e0}\right] \ . \tag{4c}$$

Energy: $$n_{\alpha 0}\left(\mathbf{V}_{\alpha 0} \bullet \nabla T_{\alpha 0}\right) + \gamma n_{\alpha 0} T_{\alpha 0} \nabla \bullet \mathbf{V}_{\alpha 0} = 0 \tag{4d}$$

In addition to the two assumptions above, two other assumptions are commonly made: 1) No equilibrium flow, and 2) Neglect the two-fluid terms (right side of Eq. 4c); i.e., only consider ideal MHD.

The first assumption allows the momentum equation (Eq. 4b) to decouple from all other equations. The momentum equation can then be written in a form called the Grad-Shafranov Equation. All linear MHD codes use this as their input. Note that in this case, the Ohm's law can be solved independently of the Grad-Shafranov equation to determine the current sources. Separate codes are usually used to determine what fraction of the current comes from Ohmic drive, bootstrap current (from the stress tensor term in Eq. 4c), Pfirsch-Schluter currents, and current drive.

Removing the first assumption, but keeping the second, allows the derivation of a modified Grad-Shafranov equation [3]. For purely toroidal flow, the modifications are rather trivial and implemented by several codes. While more accurate, these modifications are generally not included in equilibrium reconstructions because the characteristic flows in experiment are generally a quarter of the Mach speed, which gives corrections that are small compared to other uncertainties in the equilibrium reconstruction. It is hoped that as diagnostic improve, especially in determining the flow profiles, the inclusion of this term will become more routine. For flows that are both poloidal and toroidal, the modified Grad-Shafranov equation includes a singularity when the poloidal flow reaches the poloidal Alfven Mach number. Because of poloidal flow damping, poloidal flows are generally unimportant, although they may be significant near the edge. With the exception of a recent code written by a student of Betti, [4], no code in present use includes poloidal flow.

Removing all assumptions regarding equilibrium solutions has been done only recently. Inclusion of the two-fluid terms automatically requires the inclusion of the inertia term in the momentum equation to have the proper treatment of the drift flows. No code currently solves for the two-fluid equilibrium equations, nor are any initial value codes

prepared to accept two-fluid equilibria. In the future, including this capability may be important for the extended MHD codes.

B. Separation of Variables and Diffusive Sources

For the technical discussion below, we will discuss two separate modes of operation for the NIMROD code: "separated equilibrium mode" and "$n = 0$ mode". The general prescription for deriving the form of the equations solved in NIMROD is to separate the quantities into a "steady-state component" and a dynamic component: $Q(\mathbf{r},t) = Q_{ss}(\mathbf{r}) + \tilde{Q}(\mathbf{r},t)$. In all subsequent equations, the terms that contain purely steady-state factors are not explicitly included; rather, they are assumed to satisfy the constraints given by Eq. 4 and hence do not appear in the dynamical equations. *The dynamical component thus represents the deviation from the steady state solution given in Eq. 4*; it does *not* represent the total plasma state. This has implications on the interpretation of the equations. To understand this, we consider this prescription for a purely diffusive pressure equation:

$$\frac{\partial p}{\partial t} = \chi \nabla^2 p \tag{5}$$

where we assume a constant diffusivity. With homogeneous Dirichlet boundary conditions, the steady-state solution of this is *p=0.* Separating into dynamic and steady state solutions, the dynamic equation is:

$$\frac{\partial \tilde{p}}{\partial t} = \chi \nabla^2 \tilde{p} \tag{6}$$

The steady state solution is $\tilde{p} = 0$. The total pressure is $p = p_{ss} + \tilde{p} = p_{ss}$. *Note that here p_{ss} is assumed to exist and be maintained by some external mechanism.* The implication is that a source has implicitly been added to the equation. This has been the default manner in which NIMROD has run – in particular, the successful ELM milestone was performed using this method.

To understand the implications better, we want to rewrite our equation with an explicit source:

$$\frac{\partial p}{\partial t} = \chi \nabla^2 p + S_p \tag{7}$$

To derive Eq. (7), the cancellation is $S_p = -\chi \nabla^2 p_{ss}$; that is,

$$\frac{\partial p}{\partial t} = \chi \nabla^2 p - \chi \nabla^2 p_{ss} \tag{8}$$

so that $\partial p / \partial t = 0$ when $p = p_{ss}$. We term this type of source a "diffusive source" and it is can be present in all of the equations that have a diffusive term. The physical effect of the source is to maintain the equilibrium profiles. (This assumes the diffusivity is fixed.

Temperature-dependent diffusivities will have slightly different behavior). The advantage of using the sources is that for tokamak runs they approximate the real sources within a tokamak for the time-scales under consideration.

The point is that Eq. (6) (for the “dynamical” component) and Eq. (8) (for the “total” component) are mathematically equivalent. The default way for NIMROD to run tokamak simulations has been to use Eq. (6). We can solve Equation (5), which is the equivalent of Eq. (8) (informally called the “transfer eq mode” on the NIMROD team) without the sources. The M3D team uses the equivalent of Eq. (8).

C. M3D experience with Plasma Configurations with Strong Density Variations:

In a realistic plasma/vacuum situation, the plasma (charged particle) density is relatively small in the ``vacuum'' region outside the last closed flux surface that defines the confined plasma. In the edge of the plasma, the electron density falls off steeply, as does the plasma pressure. Both gradients are consistently measured in experiments. Since the pressure (or temperature) and the density evolve separately in MHD (both electron and ion temperatures in the two-fluid model), this adds to the difficulty of sustaining the original ideal MHD plasma configuration obtained from experimental reconstruction.

In the fluid model the 'vacuum' is modeled as a region of very high resistivity, which implies very low current. If the resistivity is high enough, the density in the `vacuum' can have similar magnitude to the interior density. Since the high resistivity region must also be tied to the low vacuum density in a self-consistently evolving fashion, most simulations choose to neglect the density variation altogether, as a first approximation.

We have made some preliminary trials with M3D to see what effects an edge density gradient has on the equilibrium configuration and its nonlinear stability in the resistive MHD and two-fluid descriptions. The results were limited by available computational resources, since the vacuum model was only available in an OMP (rather than MPP) version of M3D, limiting it to run on about 16-32 processors. One of the other projects of the period has been to port this to the MPP version so that it can run on hundreds or thousands of processors on Seaborg, etc.

The 2005 Q3 configuration was used as background. The full plasma, with a low resolution central region, was simulated, using 2nd order triangular finite elements. The results showed that a density profile with a relatively low density 'vacuum' region is indeed difficult to sustain. The density profile is not specified in the ideal MHD equilibrium, only the total pressure, so it was chosen to be a function of magnetic flux surface with a relatively flat central profile, falling steeply over the edge region where the pressure falls, reaching a value of 0.1 to 0.3 times the peak value outside the plasma. This is high compared to measured electron densities.

Neither the MHD nor the two-fluid equilibrium configurations could be sustained in M3D with simple sources of current and pressure, i.e., the force balance that existed in the original ideal MHD equilibrium was not maintained when the resistivity varied from

small to large over the plasma edge, as some function of plasma parameters. (A number of different resistivity schemes were tried, starting with the resistivity η proportional to $T_e^{-3/2}$). The large current spike at the edge in the steep pressure gradient region became unstable and, with the background density variation, resulted in fast movement of the plasma edge away from the equilibrium configuration. Part of the imbalance is presumably due to lack of sufficient spatial resolution, despite increasing packing of the plasma edge and vacuum region, but it appears to be worsened by having a density variation.

The usual simple sources used to maintain an ideal MHD equilibrium are not physically correct in the edge region, where strong neoclassical viscous stresses of both ions (momentum equation) and electrons (Ohm's law) actually produce the current. Their forms are not known for the time-evolving case. Applying simple forms of the neoclassical stresses, as previously used for interior plasmas, helped a little but were not sufficient. In addition, two-fluid plasma edge regions probably have strong plasma flows that are ignored by the standard MHD equilibrium reconstruction. Other kinetic effects may also contribute.

The two-fluid and MHD equilibria showed rather different instabilities. The MHD plasma edge tended to balloon toward the outboard side, strongest at the horizontal midplane. The two-fluid one tended to distort the plasma X-point, (there was a single, lower X-point). The difference is consistent with the existence of diamagnetic effects in two-fluids. The two-fluid plasma pressure perturbation tended to become large on the inboard side of the X point, where the inboard divertor is located in the experiment. This is where energy loads are observed in experimental ELM crashes, suggesting that two fluid effects may play a role once the ELM instability has distorted the plasma edge and the actual source processes enough to cause the equilibrium to change.

An example of the unstable behavior that develops when a two-fluid calculation is initialized in M3D is shown in Figure 1.

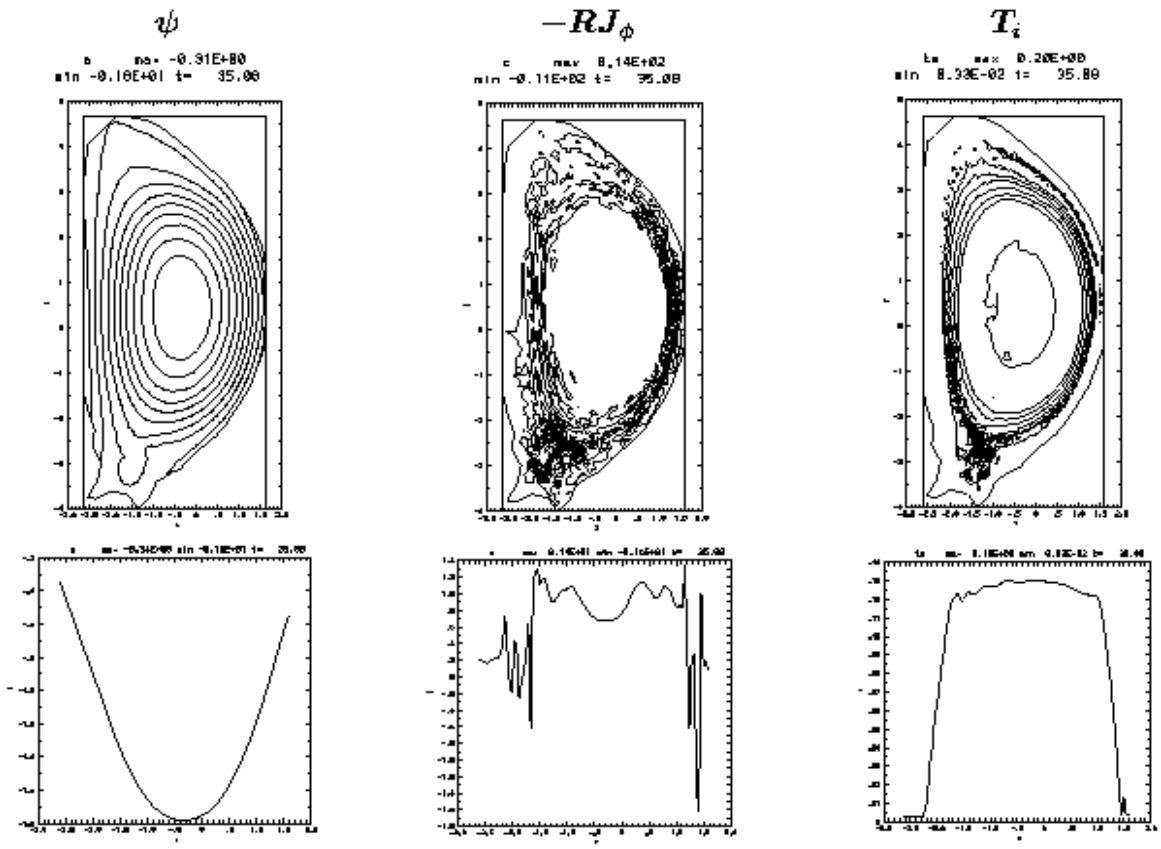

Figure 1: Contours of plasma flux (left), toroidal current density (center) and electron temperature for a M3D two-fluid run with inconsistent or inadequately resolved equilibrium.

IV. Technical Approach

A. Characterization of the Equilibrium

In this work, we only investigate the "Pedestal T_e=700 eV" equilibrium because it was the case used in the 2005 Milestone case. The results and implications of this study are generic to H-mode equilibria in general.

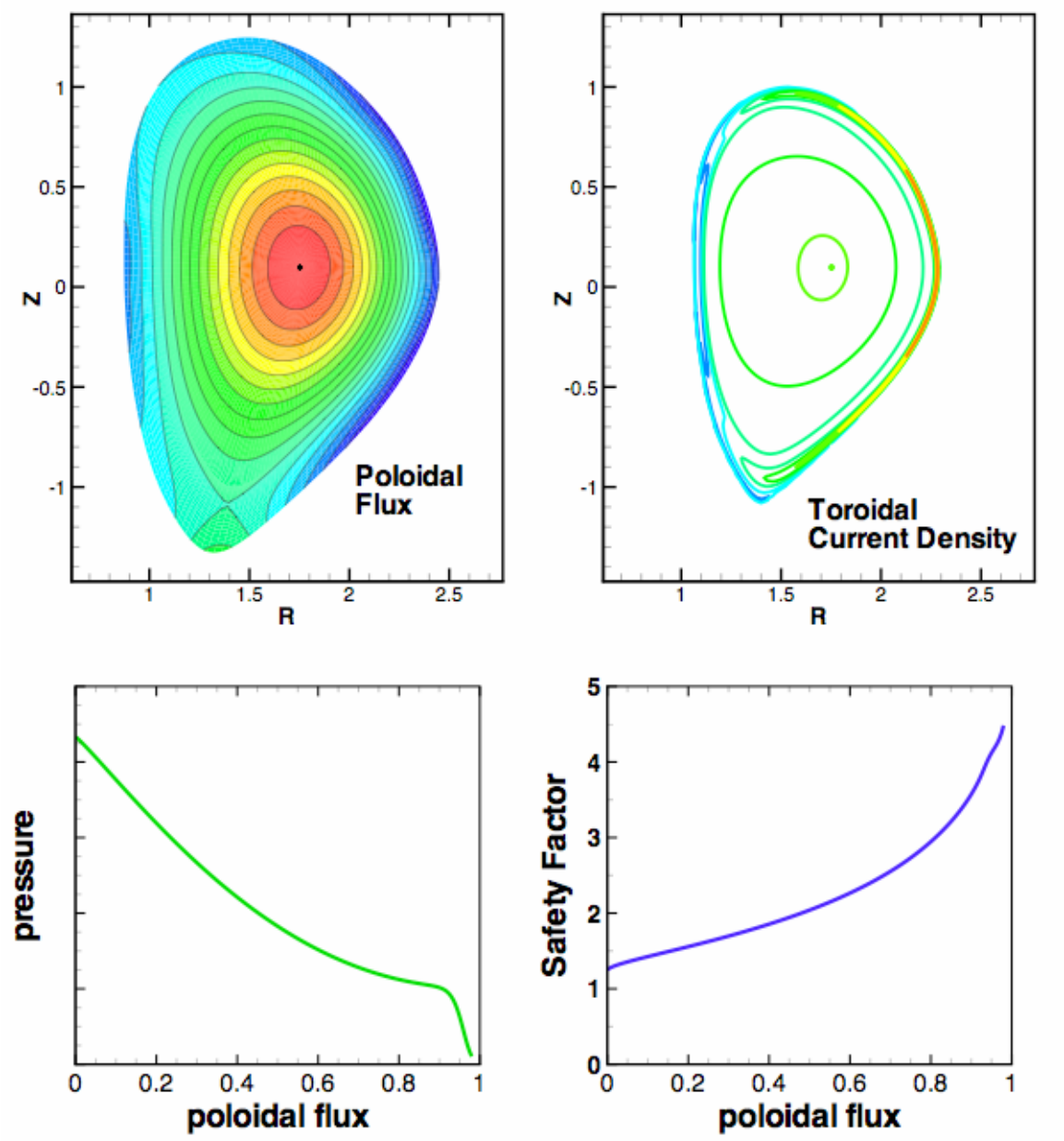

Figure 2. The equilibrium used in the 2005 Milestone report has a large localized toroidal current gradient near the separatrix, and a strong poloidal variation in the current, despite the fact that the flux surface average of the parallel current is constant.

The equilibrium is shown in Fig. 2. As shown, the current density is localized near the separatrix. Although the equilibrium was constructed such that the flux surface average

of parallel gradient (<J.B/B^2>) is zero, there are large local poloidal variations in the poloidal current. The toroidal gradient is defined to be exactly zero beyond the separatrix. Although the experiment has some finite current in the scrape-off-layer (SOL) region, at this time there is no satisfactory method to obtain those currents in such a way that the equilibrium conditions are exactly satisfied.

The effect of the sharp current gradient can be seen in the cylindrical components of the poloidal magnetic field shown in Figure 3. The sharp discontinuities at the separatrix are readily apparent. Also apparent are the rapid variations of magnetic field on the inboard side. This is caused by the existence of the poloidal magnetic field coils on the inboard side. The equilibrium codes numerically handle the coil fields using a Greene's function technique which allows them to avoid the difficulties of the fields near the coils.

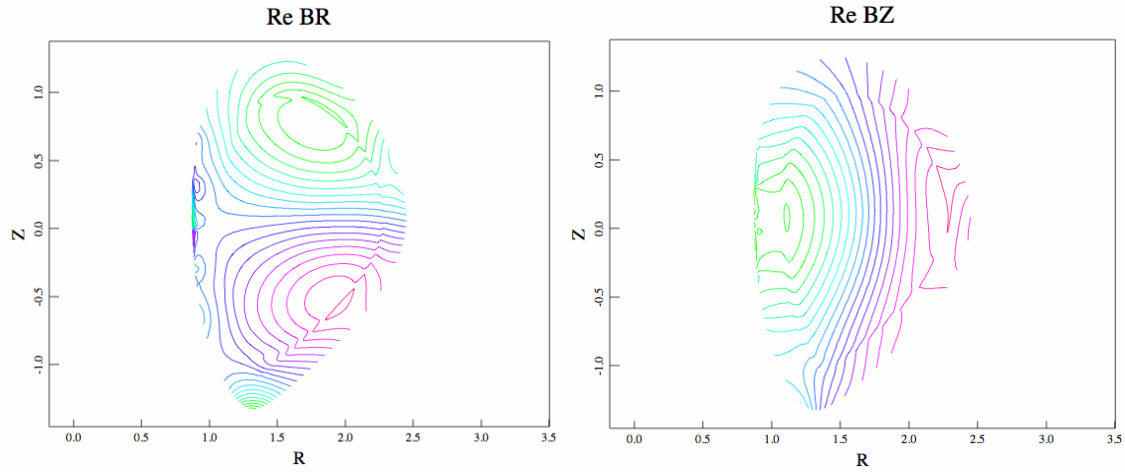

Figure 3. The cylindrical components of the magnetic field show the sharp discontinuities due to the sharp current gradients as well as the effect of poloidal field coils on the inboard side of the plasma.

As discussed in Section II.B., the 2005 Milestone simulations were run with "implicit sources". i.e., the form given by Eq. 6. Because we had no equilibrium flow, there were no momentum sources. Because we evolved only the total temperature, there was no electron pressure source. The sources were thus are a current source and a pressure source. As the equilibrium parameter plots of Figure 2 suggests, these implicit sources are highly localized. In addition to the large, localized gradients, the temperatures are low leading to large diffusivity parameters (when using Braginskii coefficients). In Figure 4, the source for the resistive Ohm's law and temperature equation are shown when Braginskii coefficients are used (for the 2005 Milestone case, the Braginskii resistivity was used for the resistive Ohm's law.). Clearly these fixed sources play an important role in the ensuing dynamics

The NIMROD runs to date have used these sources in the "separated equilibrium mode" ($Q(\mathbf{r},t) = Q_{ss}(\mathbf{r}) + \tilde{Q}(\mathbf{r},t)$) and have generally been successful. The simulations are difficult, and in this work we will investigate the extent to which the sources can cause

problems. The M3D code has performed their initial simulations by reaching a nearby steady-state using the code itself, i.e, solving Eq. 8. Our goal is to reach a similar state.

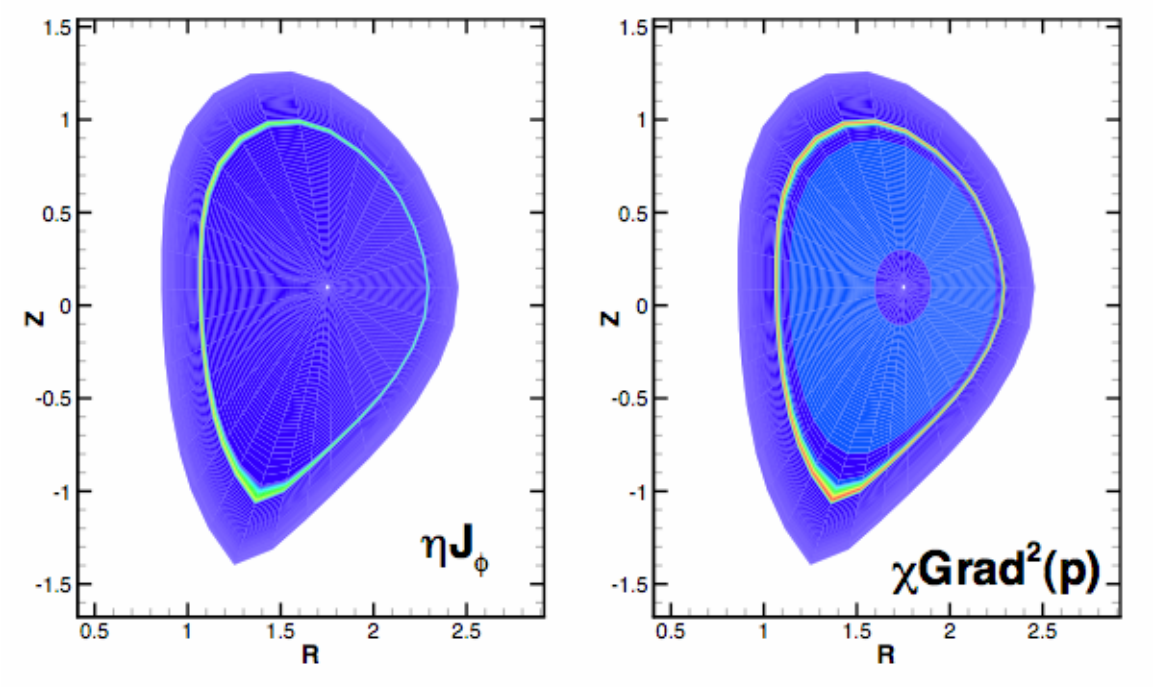

Figure 4. The diffusive sources in H-mode equilibria are very large near the separatrix when using Spitzer values. The low temperatures lead to large diffusivity values and H-mode equilibria have sharp edge pressure and current gradients.

B. Comparison of NIMROD modes of operation at low diffusivity

We are ready to discuss the $n = 0$ behavior of the ELM equilibria. We wish to study investigate the $n = 0$ behavior of the 2005 Milestone case with parameters similar to the results presented in the final report. The case has 36x40 cells with polynomial degree of 3. The temperature-dependent resistivity is evolved with a realistic $S = 1\text{x}10^8$. The peak resistivity is constrained to be 243 times the lowest resistivity. The viscosity is constant throughout the domain with a Prandtl number in the core of 6,250, and a Prandtl number in the vacuum region of 26. The viscous diffusivity and perpendicular thermal diffusivity are 25 m^2/s, and the parallel thermal diffusivity is 10^5 times larger.

We present two types of simulations: a "separated equilibrium" simulation that has implicit diffusive sources (i.e., Eq. (6)), and a "transferred equilibrium" simulation that has no source to maintain the fields (i.e., Eq. (5); in this case the "steady state" component of the solution appears only as an initial condition) . The time histories of the kinetic energy of the two runs are shown in Figure 5. As shown, after one microsecond, the energies differ by more than 13 orders of magnitude. Since we do not believe the $n = 0$ mode is inherently unstable, we conclude that *the initial "steady state" solution, as given by the Grad-Shafranov reconstruction from the experimental data, is not in sufficient force balance.*

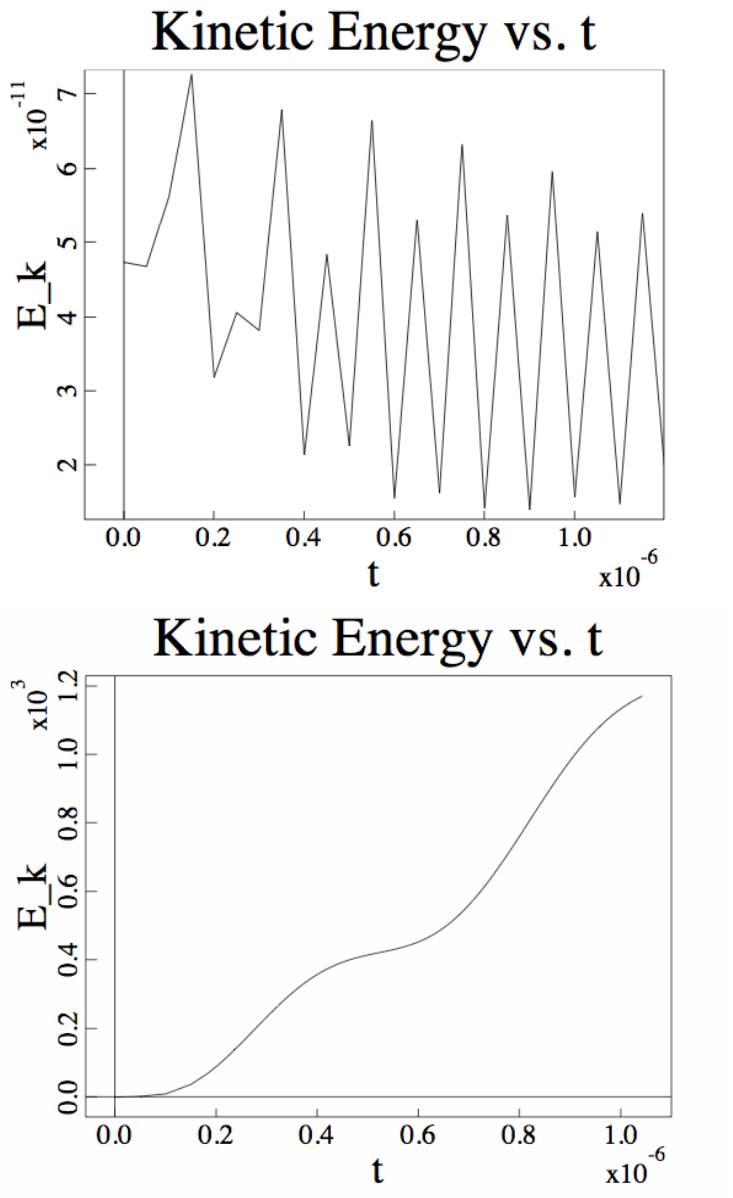

Figure 5. A comparison of two modes of NIMROD operation show a dramatic difference in behavior. The top assumes that the steady state is in exact force balance. The bottom uses the steady state as initial conditions. In one microsecond, the resultant kinetic energies differ by 13 orders of magnitude.

To explore the cause of the difficulties in the transferred equilibrium simulation (with the steady state used as initial conditions), we examine the behavior early in the time history. In Figure 6, we show plots of the radial (using major radius of the tokamak) of the velocity (because it is the largest component), and the toroidal current density (not the contravariant component). After the first time step, the current density has significant inboard current fluctuations. The reason for this is that the "equilibrium current" in this case is computed from using Faraday's law (Equation 2(b)) using the finite-element representation of the magnetic field shown in Figure 3. Because of the transfer of fields from one discretization scheme (in this case finite difference and spectral Greene's

functions) to another (a finite-element mesh), the errors manifest themselves as large toroidal current fluctuations. These toroidal current fluctuations then act to drive large flows. This is because the reconstructed solution is not in steady state on a sufficiently long time scale when transport effects are taken into account.

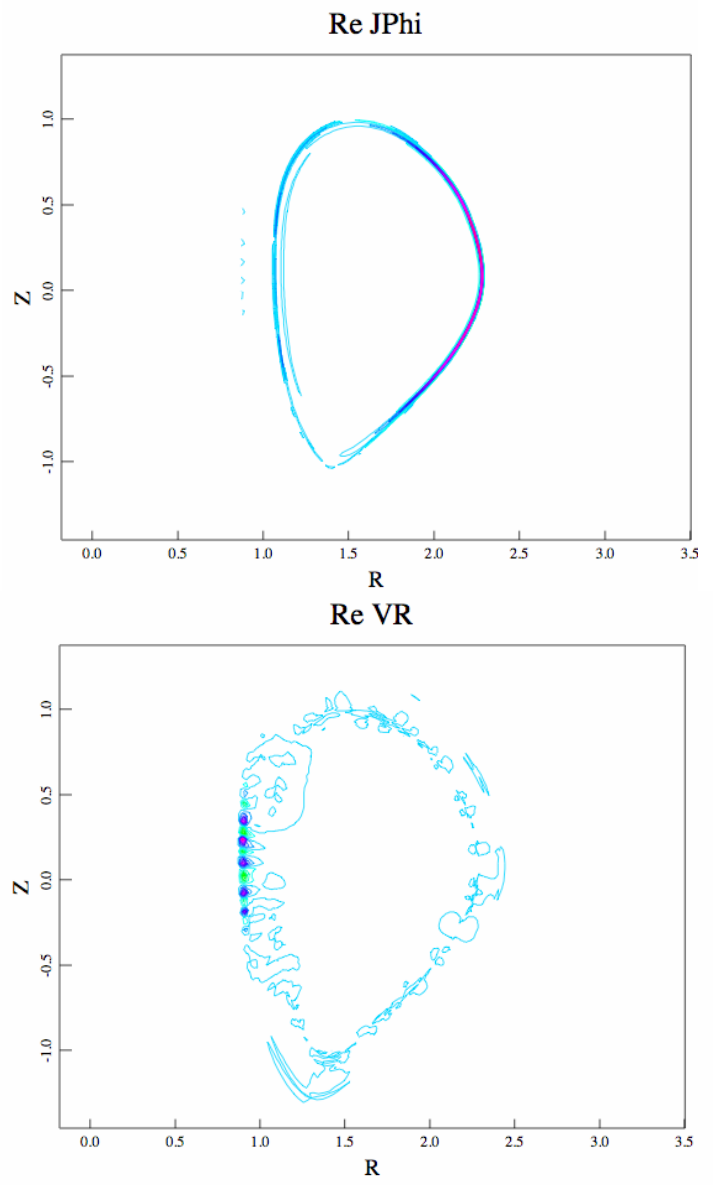

Figure 6. On the first time step, the toroidal component of the current density shows significant fluctuations on the inboard side near the poloidal flux coils. These fluctuations drive large flows on the inboard side within the first time step.

The same quantities are shown in Figure 6 after 90 time steps later (t_{sim}=9.4 x 10^{-7} sec). At this time, one can see that the induced numerical noise is beginning to broaden, and is not dominant at the edge. From both Figures 5 and 6 we note the separatrix location is clearly identified. Two sources of difficulties can be seen in these initial studies: 1) the equilibrium fields on the inboard midplane are difficult to numerically

simulate because the rapidly varying magnetic fields there, and 2) the separatrix presents its own source of difficulties.

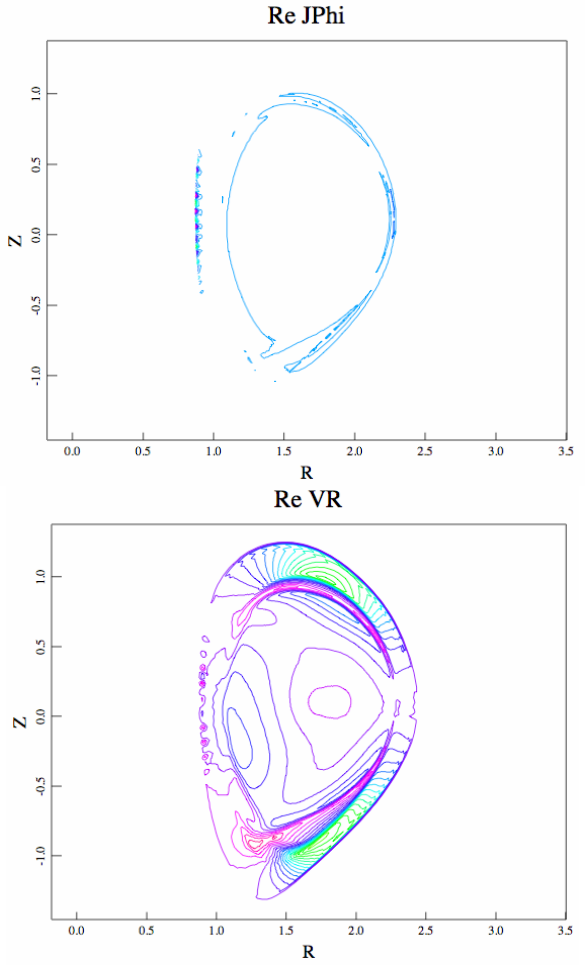

Figure 7. The velocity field begins to broaden although the difficulties with the current density still remain.

C. Development of an $n = 0$ steady-state solution in NIMROD

The typical method for developing an $n = 0$ steady-state solution for subsequent initialization is to add large diffusivities to the equations and just evolve the $n = 0$ solution to a time asymptotic steady state (referred to as "equilibrium relaxation"). This method is used by the M3D code, the TSC [5] transport code, and the HINT [6] code for three-dimensional equilibria. The advantage of this approach is that it is a robust method for finding suitable equilibria for subsequent simulation. The disadvantage is that it can complicate the analysis of the simulations when the parameters depend sensitively on the equilibria used. (The equilibria obtained from "relaxation" may differ in local detail from the original Grad-Shafranov equilibrium.)

The NIMROD code has not extensively performed simulations of this type (i.e., "relaxation") for tokamak equilibria. The goal of this work is to not only perform these types of simulations, but take advantage of NIMROD's separated equilibrium functionality and investigate its role in the development of a steady-state solution; i.e.,

why do separated equilibria work so well? The discussion of Section III.B suggests that it is because the toroidal current, which is inconsistent with the magnetic field representation in the equilibrium reconstruction, is more accurate on the inboard midplane. However, the difficulties at the separatrix also point to the existence of problems there. Do the implicit diffusive sources help in these cases?

To answer these questions, the NIMROD code was programmed to add to new capabilities: running in the transferred equilibrium mode with diffusive source (i.e., Eq. (8)), and running with the separated equilibrium mode with no sources. This gives us 4 cases to compare: with and without separated equilibrium, and with and without sources. Because of the difficulties with the current discussed above, the simulations are run at S = 1.354E+03 in the core, to be able to have the transferred equilibrium cases run and allow accurate comparisons. The viscosities are run at values of 25, 250, 2500, and 25000 m^2/s as shown in Fig 8. The thermal diffusivities are held to the same values as the cases discussed in Section III.B. Although anisotropic thermal conduction is generally considered unimportant, it was included in the simulations to ensure a proper equilibration of the n = 0 steady-state.

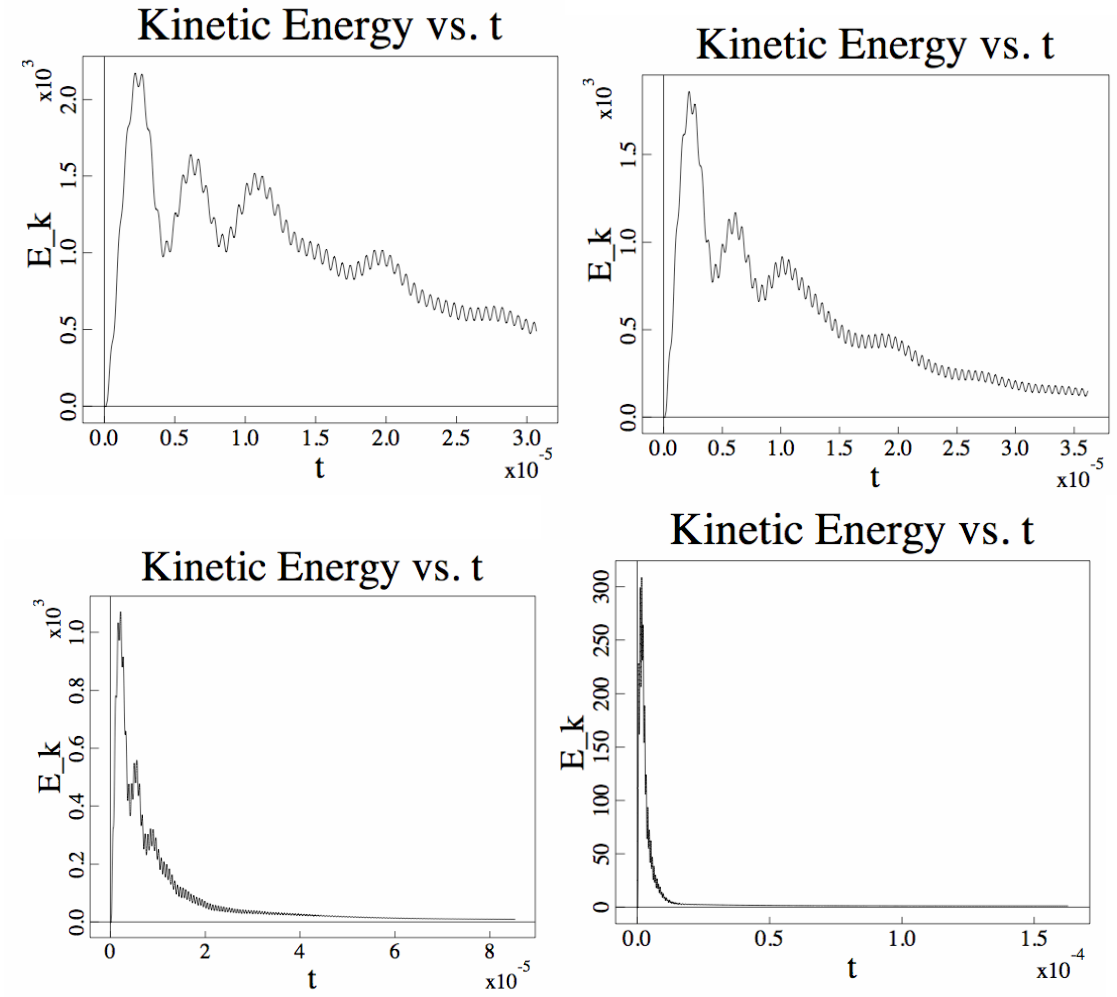

Figure 8. Time history plots for the transferred equilibrium case with sources for kinematic viscosities of 25, 250, 2500, and 25,000 m^2/s.

We first discuss the transferred equilibrium cases. The time history plots for the cases with and without sources are quantitatively similar. For simplicity, only the time history plots for the case with sources are shown. The peak kinetic energy and decay time corresponds to the magnitude of the viscosity as one would expect. The two highest cases have clearly reached an $n = 0$ steady-state as shown.

The types of steady state reached are different. Considering only the largest viscosity for simplicity, we compare the toroidal current and magnetic field in Figure 9. As expected, the case that has a source acting to maintain the equilibrium has a steady-state that is closer to the original equilibrium. The case without sources has smoother fields.

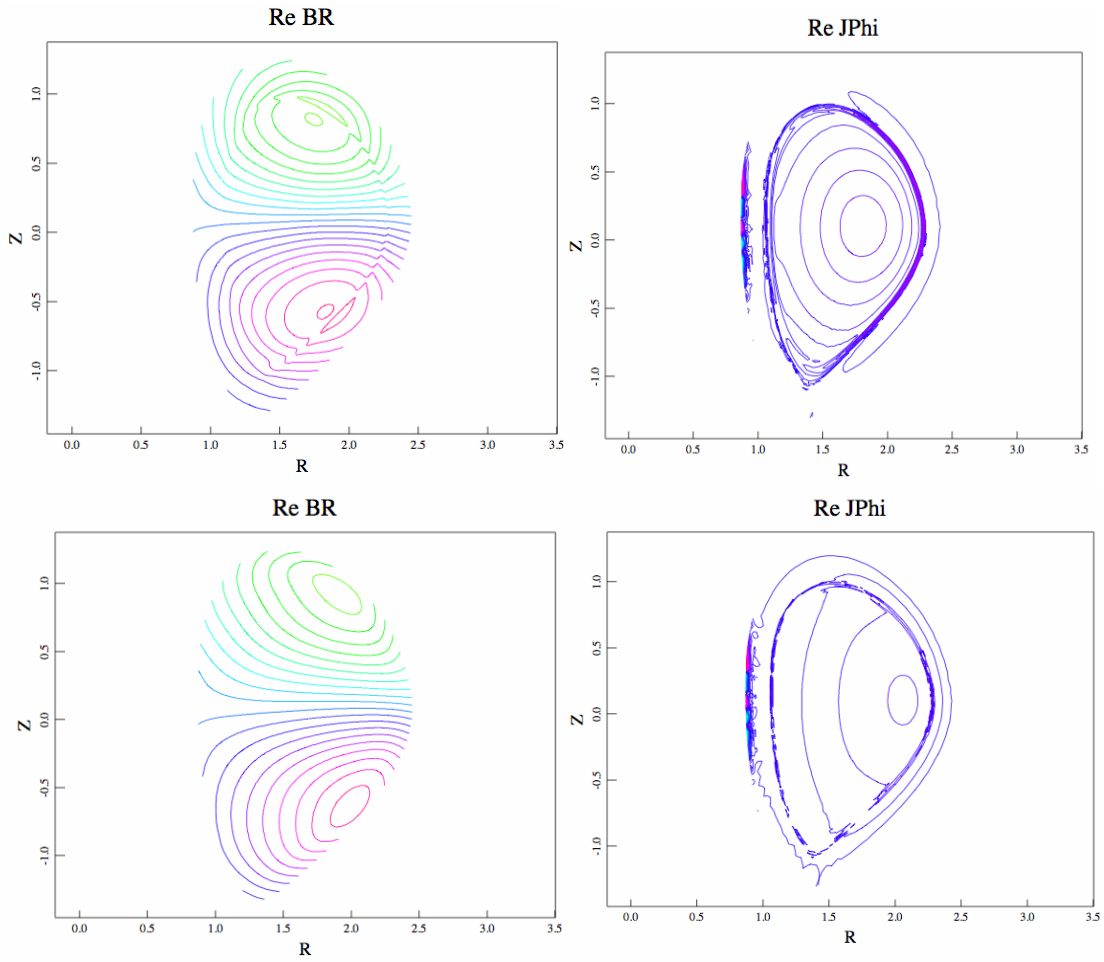

Figure 9. A comparison of the transferred equilibrium cases with sources (top) and without sources (bottom). The magnetic field for the case with sources looks similar to the magnetic field shown in Fig. 2 unlike the case without sources.

The separated equilibria cases have much different behavior. We first consider the typical NIMROD run which has the implicit diffusive sources. All of the cases with the various viscosities have a similar time history plots with the kinetic energy never rising above 10^{-10} Joules. With such small changes, there are essentially no discernible differences in the equilibria from what has been shown in Figures 2 and 3, so they will not be shown.

The case of separated equilibria with no sources shows some interesting differences from the equilibrium cases. As one would expect, the plasma evolves to move away from the having the sharp gradients, with the time scale corresponding to the viscosity time scale. The time history plots of the kinetic energy are shown for two viscosity cases in Figure 10. After relatively fast transients, the plasma evolves on a transport time scale as expected. For the highest viscosity case shown in Figure 11, the current density peak is slightly broader than previous cases as one would expect. The overall magnetic field differs a little from the equilibrium magnetic field, but not significantly.

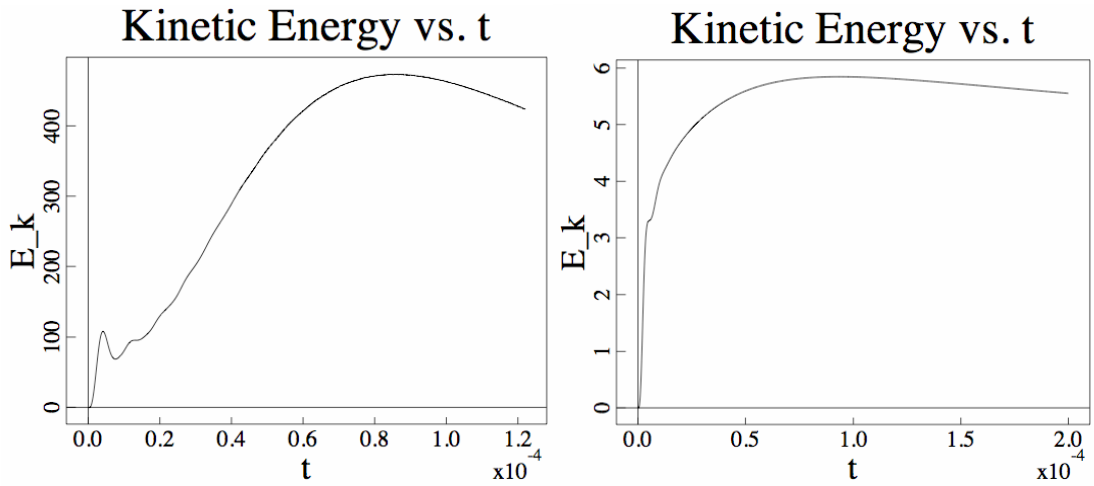

Figure 10. The time history plots of the kinetic energy for the separated equilibrium case with no sources for the viscosities of 250 (left) and 25,000 (right).

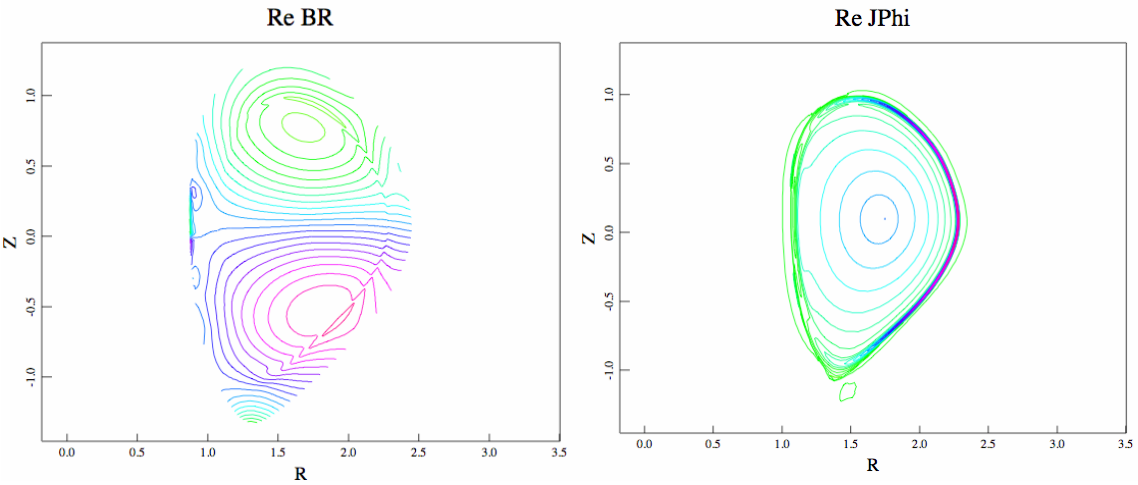

Figure 11. The torodial current density and magnetic field are very similar to the equilibria, but slightly broader. The current extends into the open field region slightly.

D. Resolution Requirements for Two Fluid ELM Simulations with M3D: Background and new Developments

In FY05, two-fluid ELM simulations with M3D focused on the stabilizing effect of gyro-viscosity. The size of the two fluid effects is measured by the Hall parameter H, the ratio of the ion skin depth to the major radius. Two fluid stabilization provides a cutoff scale below which MHD modes are stable.

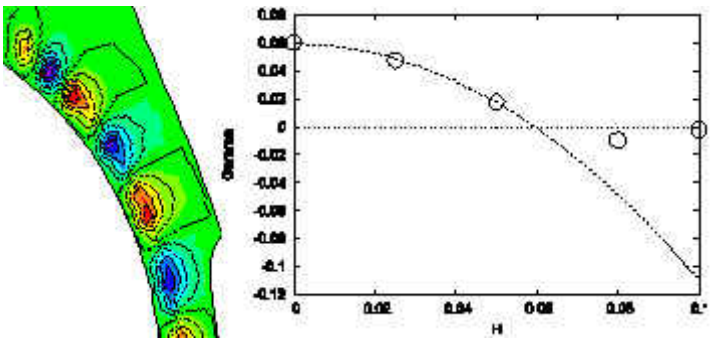

Figure 12: Contours of electrostatic potential (left) and ELM growth rate as a function of the Hall parameter H.

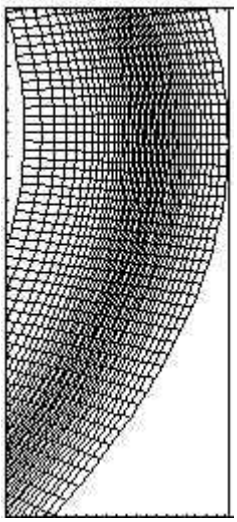

Figure 13: Zones in M3D are packed near the pedestal region.

Hence two fluid effects were shown to have an important role in setting the spatial scale of ELMs. The gyroviscous stabilization of MHD instabilities scales as nH. This was verified in linear simulations of n=10 ballooning modes in the edge of a DIIID equilibrium, shown in Figure 12. On the left are contours of electrostatic potential in a part of a magnetic flux tube on the outer part of the equilibrium. On the right is the instability growth rate as a function of the Hall parameter H (varied from 0 to 0.1). It is seen that the growth rates decrease with H and are stable for a critical value H = 0.06.

In attempting nonlinear simulations of these modes, it became clear that it is necessary to have adequate resolution of the higher toroidal modes generated in the simulation. Nonlinear calculations thus require much more resolution than do linear simulations of a single toroidal mode. The focus of this quarter was to develop grid-packing and other techniques to adequately resolve the structures that develop in the non-linear ELM simulatilons. An example of a section of the new mesh is shown in Figure 13. With this mesh, the pedestal edge pressure gradient and equilibrium current spike which coincides with the pedestal are well resolved. There

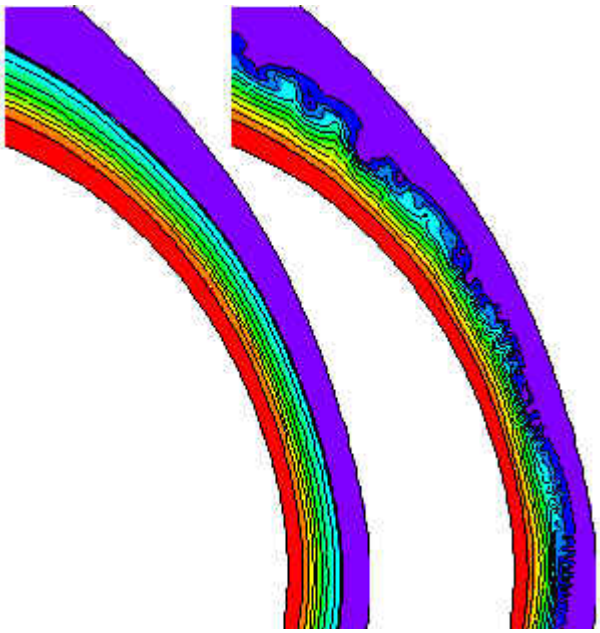

Figure 14: Equilibrium pressure gradient (left) and pressure contours in a nonlinear simulation in a M3D calculation.

should be even more poloidal resolution to resolve the nonlinear structures shown in Figure 14. The first part of the figure shows the equilibrium pressure gradient. To the right are pressure contours in a nonlinear simulation. This simulation has toroidal modes n = 4, 8, … 20. In this particular simulation H = 0, but other simulations are being done with nonzero H, to assess its effect.

In the above cases, the initial equilibrium was taken from a DIII-D equilibrium (the tq3 case). In future work, we will try to use initial pressure profiles calculated by the XGC neoclassical kinetic code [7].

E. Development of Self Consistent Stationary H-Mode Equilibrium with TSC

Another approach for obtaining stationary steady state equilibrium is to use the axisymmetric TSC code [3] to simulate the free-boundary resistive time scale evolution of an H-mode discharge into the "stationary" part of the discharge when the magnetic fields are not changing in time. This should provide an equilibrium state with density, pressure, and current profiles that are consistent with an Ohmic current profile with a self-consistent bootstrap current imposed.

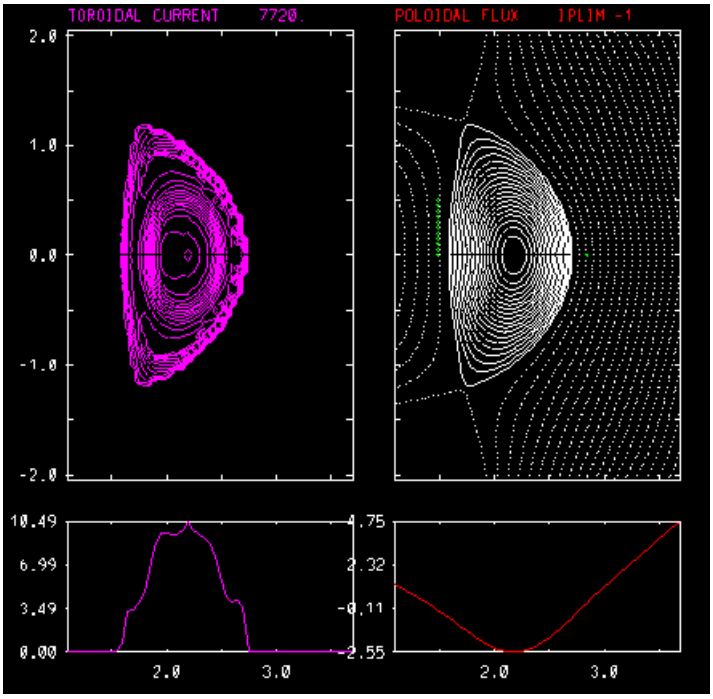

Figure 15: Current and flux contours in the stationary phase of the proposed FIRE experiment

In the TSC code, the plasma evolves through a series of equilibrium states in which the Grad-Shafranov equation is satisfied. The rotational transform ι (the inverse of the safety factor q) evolves relative to the toroidal flux Φ according to the one dimensional evolution equation:

$$\frac{\partial}{\partial t}\iota = \frac{\partial}{\partial \Phi} V_L \qquad (9)$$

Where the local loop voltage, a surface quantity, is given by:

$$V_L(\Phi) = \frac{2\pi \left\langle \vec{E} \bullet \vec{B} \right\rangle}{\left\langle \vec{B} \bullet \nabla \phi \right\rangle} \qquad (10)$$

Here $\vec{E}$ and $\vec{B}$ are the local electric and magnetic fields, and ϕ is the symmetry angle. The parallel electric field is given by a parallel Ohm's law, and is of the form:

$$\left\langle \vec{E} \bullet \vec{B} \right\rangle = \eta_{\parallel} \left\langle (\vec{J} - \vec{J}_{BS} - \vec{J}_{RF} - \vec{J}_{NB}) \bullet \vec{B} \right\rangle . \qquad (11)$$

Here, the current terms in the bracket refer to the total current density, the bootstrap current density, the RF driven current, and the neutral-beam driven current. In the stationary phase of a discharge, Equation (9) has come to a steady state, and the current density is determined by different source terms in Equation (11), which are transport model dependent.

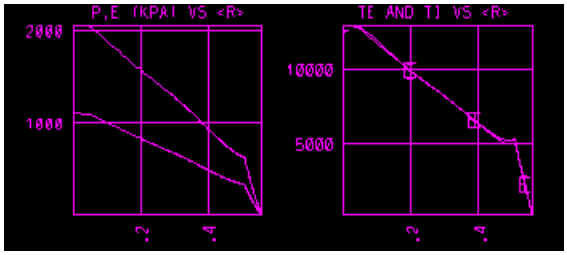

Figure 16: Total and Electron pressure (left) and temperature profiles in FIRE

The stationary equilibrium we have been examining corresponds to the end of the flattop phase of the proposed FIRE experiment. The flux and current contours are shown in Figure 15. We show the corresponding pressure and temperature and current density profiles in Figures. 16 and 17.

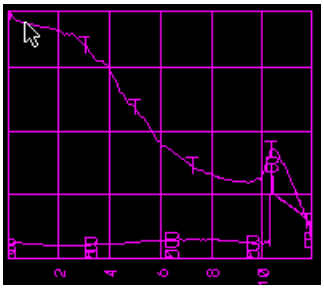

Figure 17: Total (T) and Bootstrap (B) current densities in a FIRE simulation

We have developed techniques to converge these stationary equilibrium to high-accuracy stationary equilibrium, which can then be transferred to M3D and/or NIMROD. An advantage of this technique is that the TSC code treats the vacuum region near the plasma as a high-resistivity region, as do NIMROD and M3D. This implies that all quantities are continuous across the separatrix boundary, a fact which should facilitate the transfer of equilibrium quantities. This technique will also be used in the SWIM project. We are presently obtaining detailed shot information on a typical stationary H-mode shot on DIII-D for which to apply this method.

We expect that the stationary equilibrium, so obtained, will be very close to equilibrium in the NIMROD and M3D code if the sources are transferred accurately as well, and if the resistive MHD model is used. However, it is predicted that for the 2-fluid Extended MHD model, these zero-velocity stationary equilibrium will be unstable to a poloidal spin-up, but that there will be a nearby stable stationary equilibrium with flow. Our present focus is to obtain this nearby stable equilibrium with a relaxation technique as described in Section C above.

V. Conclusions

It is clearly shown that there are difficulties in the standard way of constructing initial equilibrium for ELM studies for both NIMROD and M3D. Nearby, $n = 0$ steady state solutions for the NIMROD code have been found using two different numerical methods under two different simulation conditions: with and without sources. The quality of the "separated equilibrium mode" greatly surpasses that of the "transferred equilibrium mode", and in the near term is likely to be the preferred method of running NIMROD. The development of the code to allow for each mode of operation to include or neglect the sources is beneficial to performing these types of studies and has greatly increased the flexibility of the code.

In this work, the primary focus was on creating an $n = 0$ steady-state that can be used to create a well-posed initial condition for the nonlinear simulations. The larger question is what is the right initial condition for studying the physics we want. To date, the equilibria have primarily been chosen based on its linear MHD stability properties. As we move forward, we will need more information from transport codes so that all of the profiles can simultaneously satisfy the steady-state condition as discussed in Section IV-E above.

Although we state transport code information is needed, we note in passing that the ability to work with high-quality free-boundary equilibria is crucial. To date, the NIMROD and M3D codes have been getting free-boundary equilibria from the EFIT and TEQ codes without much regard for the transport properties. A method for transferring the equilibrium information from TSC (or other free-boundary transport codes) needs to be further developed and interfaces from those codes to NIMROD and M3D will need to be defined. The question of the axisymmetric stability of the zero-velocity stationary equilibrium needs to be explored, as discussed in Ref. [8] below.

The M3D code has demonstrated the stabilizing effect of gyroviscous terms for the ELM, and also the need for extreme resolution near the plasma boundary, which they obtain with mesh packing.

This work was supported by the U.S.D.O.E.

References:

[1] Sovinec, C.R., Glasser, A.H., Gianakon, G.A., et al, J. Comput. Phys. 195 (2004) 355
[2] Park, W., Belova, E.V., Fu, G.Y., Tang, X.Z., Strauss, H.R., Sugiyama, L.E., Phys. Plasmas 6, 1796 (1999)
[3] Hameiri, E. Physics of Fluids **26** 230 1983
[4] Guazzotto L, and Betti R, Phys. Plasmas **12** 056107 (2005)
[5] Jardin, S.C., Pomphrey, N. and DeLucia, J, J. Comput. Phys **66** 481 (1986)
[6] Harafugi, Hayashi T., and Sato T., J. Comput. Phys **81**, 169 (1989)
[7] Chang, C.S., Ku, S., and Weitzner, H., Phys. Plasmas **11**, 2649 (2004)
[8] Rosenbluth M.N and Taylor JB, Phys. Rev. Lett **23** 367 (1969)